

Huntingtin Associates with Acidic Phospholipids at the Plasma Membrane*

Received for publication, April 4, 2005, and in revised form, July 15, 2005 Published, JBC Papers in Press, August 5, 2005, DOI 10.1074/jbc.M503672200

Kimberly B. Kegel^{†1}, Ellen Sapp[‡], Jennifer Yoder[‡], Benjamin Cuiffo[‡], Lindsay Sobin[‡], Yun J. Kim[‡], Zheng-Hong Qin[‡], Michael R. Hayden[§], Neil Aronin[¶], David L. Scott^{||}, Gerhard Isenberg^{**}, Wolfgang H. Goldmann^{†‡}, and Marian DiFiglia[†]

From the [†]Department of Neurology, Massachusetts General Hospital, Charlestown, Massachusetts 02129, [§]Molecular Medicine and Therapeutics, University of British Columbia, Vancouver, British Columbia V5Z-4H4, Canada, the [¶]Department of Medicine and Cell Biology, University of Massachusetts Medical School, Worcester, Massachusetts 01655, ^{||}Renal Unit, Massachusetts General Hospital, Charlestown, Massachusetts 02129, ^{**}Biophysics Department, Technical University of Munich E22, Garching 85747, Germany, and ^{†‡}Zentralinstitut für Biomedizinische Technik, Universitaet Nuernberg-Erlangen, Erlangen D-91052, Germany

We have identified a domain in the N terminus of huntingtin that binds to membranes. A three-dimensional homology model of the structure of the binding domain predicts helical HEAT repeats, which emanate a positive electrostatic potential, consistent with a charge-based mechanism for membrane association. An amphipathic helix capable of inserting into pure lipid bilayers may serve to anchor huntingtin to the membrane. In cells, N-terminal huntingtin fragments targeted to regions of plasma membrane enriched in phosphatidylinositol 4,5-bisphosphate, receptor bound-transferrin, and endogenous huntingtin. N-terminal huntingtin fragments with an expanded polyglutamine tract aberrantly localized to intracellular regions instead of plasma membrane. Our data support a new model in which huntingtin directly binds membranes through electrostatic interactions with acidic phospholipids.

Huntingtin (htt)² exists predominantly in the cytoplasm as a soluble protein that associates with the plasma membrane and multiple membranous organelles and vesicles (1–3). Many htt binding partners function in membrane trafficking (4). A specific molecular function for htt at membranes has not been demonstrated. The large size of htt (348 kDa) and interactions with numerous membrane-associated proteins suggest that htt may function as a scaffold.

A polyglutamine expansion in the N terminus of htt (N-htt) causes neurodegeneration in Huntington disease (HD) and accumulation of htt in neurons. Degradation pathways for htt include endosomal-lysosomal and autophagic pathways and may require targeting to membranes to initiate clearance (5, 6). Therefore, knowledge of the effects of

polyglutamine expansion on htt membrane targeting is important for understanding HD pathogenesis.

N-htt has a membrane association domain. Membrane fractions prepared from control and HD brains (7) or prepared from cells expressing exogenous htt (5) contain N-htt fragments (~440–550 aa). *In vitro* translated normal and mutant htt (aa 1–548) localized to vesicles in extruded squid axoplasm (8). The structural features that mediate membrane association of N-htt are unknown and could include a proline-rich Src homology 3-binding domain that lies immediately distal to the polyglutamine stretch and HEAT domains, which are repeated regions of low homology shared by huntingtin with elongation factor 3, the p65 regulatory A subunit of protein phosphatase 2A, and TOR1 and a host of other proteins (9). The function of HEAT domains is unknown, but these repeated regions are leucine-rich and predicted to be α -helical in nature, with each repeat consisting of two helices and a short intervening linker. Crystallography studies of the protein phosphatase 2A p65 regulatory subunit (PR65/A) indicate that its multiple HEAT domains create a superhelical structure (10). htt has three domains at aa 205–329, 745–942, and 1534–1710 containing a total of 10 HEAT repeats (9).

In this study, we identify sequences in N-htt important for binding to membranes, explore mechanisms by which this binding occurs, and investigate the effect of polyglutamine expansion in N-htt membrane targeting.

MATERIALS AND METHODS

Cell Culture and Transfections—COS-1 cells (monkey epithelial) and MCF-7 cells (human epithelial) (each obtained from American Type Culture Collection) and X57 (mouse immortalized clonal striatal cells (11)) were cultured and transfected as previously described (5, 12).

Immunofluorescence, Confocal Analysis, and Cell Counting—Immunostaining and confocal microscopy was performed as previously described using paraformaldehyde fixation (5, 12). Individual images for each excitation wavelength (405, 488, or 568 nm) were obtained sequentially using a Bio-Rad Radiance 2100 confocal laser with krypton-argon and blue diode lasers through a 100 \times Nikon Plan Apo objective (numerical aperture 1.4) with oil immersion on an inverted Nikon Eclipse TE300 fluorescent microscope. Concentrations for primary antibodies were as follows: anti-htt Ab 1 (1 μ g/ml) and Ab 585 (1:1000) (1); anti-FLAG mAb M5 (10 μ g/ml; Sigma). Secondary antibodies were used at 1:1000 and included Cy3 conjugates (Jackson ImmunoResearch, West Grove, PA) and Bodipy FL conjugates (Molecular Probes, Inc., Eugene, OR). Analyses were performed using a \times 60 oil objective by an examiner unaware of the experimental conditions. 100 transfected cells

* This work was supported by National Institutes of Health Grants NS16367 and NS35711 (to M. D.) and NS38194 (to N. A.), a grant from the Huntington's Disease Society of America Coalition (to M. D.), a grant from the Hereditary Disease Foundation (to K. B. K.), and Deutsch Forschungsgemeinschaft Grant Is 85/-1 and NATO (to W. H. G.). The costs of publication of this article were defrayed in part by the payment of page charges. This article must therefore be hereby marked "advertisement" in accordance with 18 U.S.C. Section 1734 solely to indicate this fact.

The amino acid sequence of this protein can be accessed through NCBI Protein Database under NCBI accession numbers NP_002102, P51111, BAA36752, P42859, AAC63983, and P5111.

¹ To whom correspondence should be addressed: Dept. of Neurology, MA General Hospital East, 114 CNY 16th St., Rm. 2125, Charlestown, MA 02129. Tel.: 617-726-8446; Fax: 617-726-1264; E-mail: kegel@helix.mgh.harvard.edu.

² The abbreviations used are: htt, huntingtin; HD, Huntington disease; HIP, huntingtin interactor protein; N-htt, N-terminal htt; PH, pleckstrin homology; PI, phosphatidylinositol; PI(4,5)P₂, phosphatidylinositol 4,5-bisphosphate; PLC, phospholipase C; PR65/A, p65 regulatory A subunit; PM, plasma membrane; aa, amino acid(s); Ab, antibody; mAb, monoclonal antibody; ANOVA, analysis of variance; GST, glutathione S-transferase.

per coverslip were counted on three coverslips per condition ($n = 3$). Transfected cells were scored positive if >50% of the plasma membrane had labeling when viewed through a cross-section containing the nucleus. Statistical significance was determined using ANOVA and a *post hoc* Bonferroni test using Graphpad InStat software. For neomycin treatment, transfected cells on coverslips were treated with 10 mM neomycin sulfate (Sigma) in complete medium for 18 h prior to fixation. At least 200 transfected cells per coverslip were scored for >50% patchy plasma membrane (PM) staining on four coverslips per condition ($n = 4$). For transferrin uptake, cells were washed twice with Dulbecco's modified Eagle's medium 24 h after transfection and then incubated with 5 $\mu\text{g/ml}$ tetramethyl rhodamine transferrin (Molecular Probes) in Dulbecco's modified Eagle's medium at 37 °C for 15 min. Cells were washed twice with phosphate-buffered saline prior to fixation with paraformaldehyde and then immunostained for FLAG as described above. Internalized transferrin was quantified by scoring cells with >10 transferrin-positive spots visible within the cell body using a 60 \times oil objective (25 transfected cells and 25 untransfected cells per coverslip, four coverslips). Statistical significance was determined using a two-tailed Student's *t* test. As a control protein, c-Jun N-terminal kinase-interacting protein 1, which acts as a scaffold for c-Jun N-terminal kinase and other members of mitogen-activated protein kinases (13), was used.

Plasmids—Plasmids encoding FLAG-huntingtin fusion proteins in pcDNA3 have been previously described (5, 12). The addition of the FLAG epitope tag to the N terminus of htt does not affect the cytoplasmic localization of expressed htt in cells (12) or normal htt function in a knock-in mouse model.³ The numbering of the amino acids is based on wild-type htt with 23 glutamines. All new plasmids with cDNA inserts were constructed using standard subcloning techniques and PCR. For H172–448-GFP, an htt PCR product was cloned into pEGFP-N1 (BD Biosciences Clontech) preceding green fluorescent protein (GFP). The Promega GeneEditor *in vitro* site-directed mutagenesis system (Madison, WI) was used to introduce mutations. GST expression plasmids encoding GST-htt fusion proteins were made using pGEX-3X expression vector (Amersham Biosciences) and complementary synthetic oligonucleotides corresponding to segments of htt flanked by BamHI and EcoRI restriction sites. The presence of all inserts and mutations was confirmed by DNA sequencing.

Subcellular Fractionation and Western Blot Analysis—Subcellular fractionations, SDS-PAGE, and Western blot analysis were performed as described previously (5). Briefly, cell homogenates made in 10 mM HEPES, pH 7.4, 250 mM sucrose, 1 mM EDTA plus protease inhibitors were centrifuged at 2000 $\times g$ to obtain the crude nuclear pellet (P1) and the postnuclear supernatant (S1). S1 was again centrifuged at 100,000 $\times g$ to obtain the membrane pellet (P2) and the cytosolic fraction (S2). Lanes were loaded with 10 μg of protein from each fraction. Distribution of the transmembrane protein calnexin (an endoplasmic reticulum marker) was used to assess the purity of fractions. For Western blotting, the following concentrations of antibodies were used: anti-htt Ab 1 (0.5 $\mu\text{g/ml}$), anti-htt mAb 2166 (1:1000; Chemicon), and anti-calnexin (1:1000; Stressgen). Peroxidase-labeled secondary antibodies (Jackson ImmunoResearch) were diluted 1:5000. Blots were developed using ECL (Amersham Biosciences). Densitometry data from at least three separate experiments were analyzed using SigmaScan (Jandel); where a doublet was observed at the appropriate relative molecular mass, both bands were measured. Statistical significance was determined using an ANOVA and *post hoc* Bonferroni tests (Graphpad InStat).

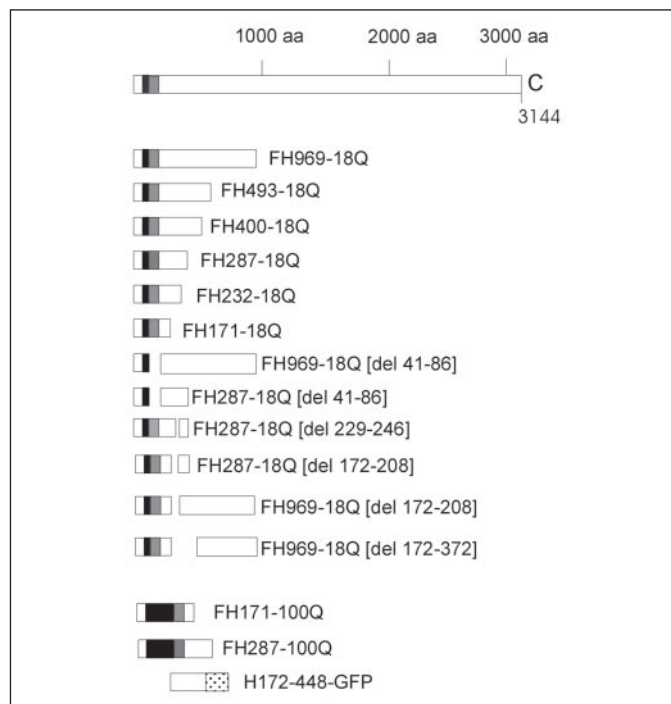


FIGURE 1. Constructs used in this study. For each construct, *F* indicates FLAG epitope tag, *H* indicates htt sequence starting from aa 1 to the number indicated, *-18Q* or *-100Q* indicates polyglutamine length (normal and mutant), and *del* indicates deletion of the aa listed. The polyglutamine stretch is black, and the polyproline region is gray. Full-length htt is shown at the top. Stippled box, GFP.

Immunoprecipitation—Immunoprecipitations were performed as described (14) using anti-FLAG mAb M2-Sepharose (Sigma). Western blots were probed with anti-htt interactor protein 1 (anti-HIP1) monoclonal antibody (Signet Pathology Systems, Dedham, MA) or anti-htt Ab 1.

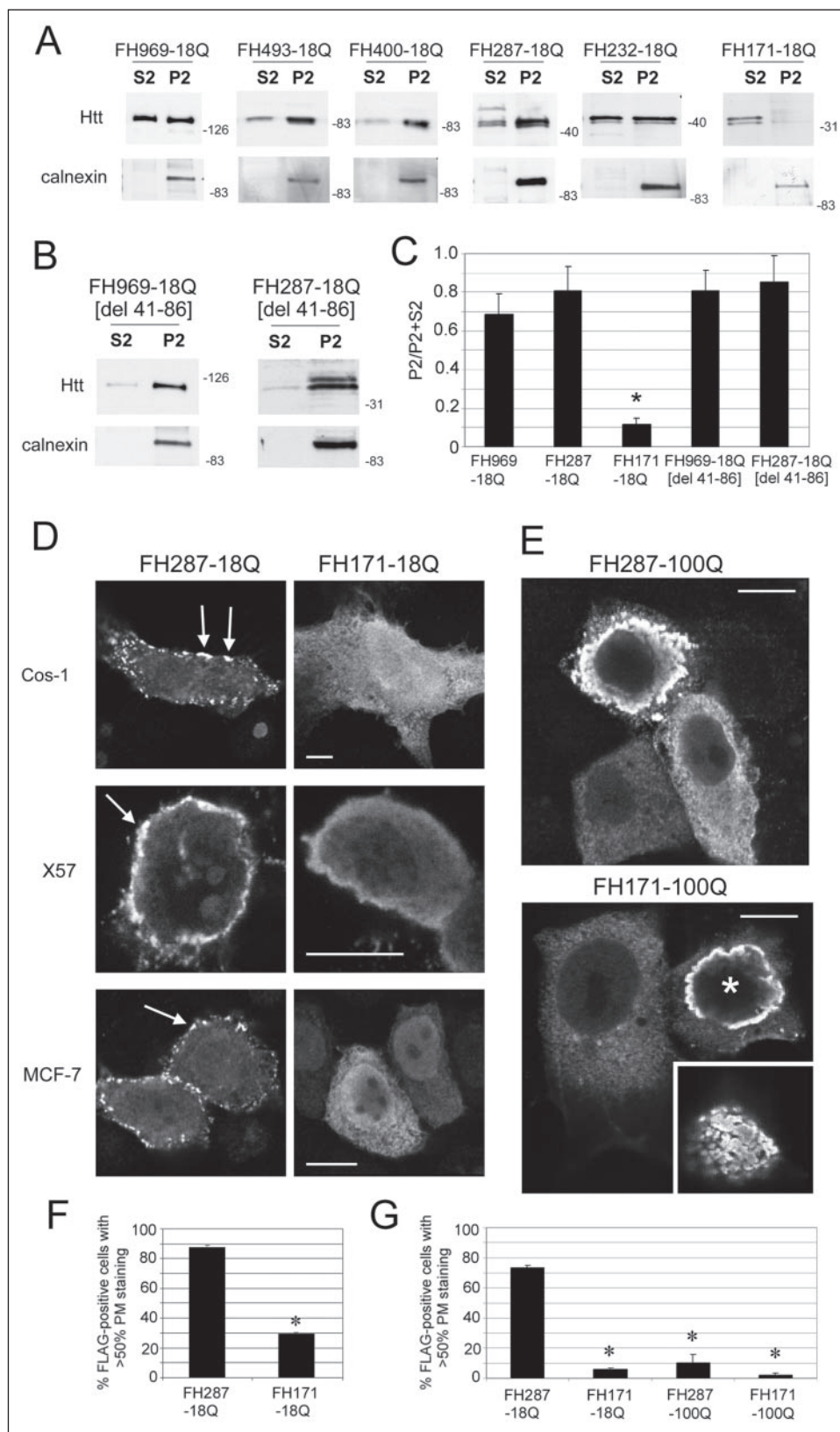
Production and Purification of GST-Peptide Fusion Proteins—Bacterial clones (*Escherichia coli* BL21 Gold, Stratagene, La Jolla, CA) expressing various peptides in pGEX-3x (Amersham Biosciences) were grown in 2 YT broth and induced with isopropyl 1-thio- β -D-galactopyranoside. GST fusion protein was purified using a bulk GST purification module (Amersham Biosciences). Proteins were dialyzed into buffer (20 mM HEPES/NaOH, 1 mM EGTA, 1 mM EDTA, 0.2 mM dithiothreitol, and 40 mM NaCl at pH 7.4) prior to use in calorimetry assays. Purity of the GST fusion proteins was determined by SDS-PAGE and Coomassie staining.

Differential Scanning Calorimetry—The phospholipids dimyristoyl-L- α -phosphatidylcholine and dimyristoyl-L- α -phosphatidylglycerol were purchased from Avanti Polar Lipids (Birmingham, AL). The experimental buffer consisted of 20 mM HEPES/NaOH, 1 mM EGTA, 1 mM EDTA, 0.2 mM dithiothreitol, 40 mM NaCl, and 0.005% NaN_3 at pH 7.4. Lipid stock solutions were prepared by dissolving pure crystalline phospholipids or mixtures of crystalline phospholipids (dimyristoyl-L- α -phosphatidylcholine, dimyristoyl-L- α -phosphatidylglycerol) in chloroform/methanol, 2:1 (v/v); lipid vesicles (200-nm diameter) were prepared by pressing a prepared lipid dispersion 10 times through two (stacked) 200-nm Nucleopore polycarbonate filters of an extruder (Lipex, Canada). All extrusion procedures were conducted at least 10 °C above the gel-liquid-crystal transition temperature (15). Calorimetric measurements were carried out in a Microcal MC-2 unit (Microcal Inc., Amherst, MA) prior to the equilibration of the sample at 4 °C for 30 min. Differential scanning calorimetry samples (1.5 ml) containing 1.5 mg of lipids, with or without GST fusion proteins, were then injected into the

³ S. O. Zeitlin, personal communication.

Huntingtin Associates with Acidic Phospholipids

FIGURE 2. Biochemical and immunocytochemical analysis of expressed N-htt constructs. *A*, Western blots of subcellular fractions S2 (100,000 × *g* supernatant) and P2 (100,000 × *g* pellet) from COS-1 cells expressing huntingtin deletion constructs. htt was detected with polyclonal antibody Ab 1 for all constructs except FH969-18Q, which was detected with mAb 2166. Distribution of calnexin (an endoplasmic reticulum marker) shows purity of fractions. Molecular mass in kDa is indicated to the right. 10 μg of protein was loaded per lane. *B*, S2 and P2 fractions from cells expressing constructs bearing the polyproline deletion. FH969-18Q (del 41–86) was detected with mAb 2166. FH287-18Q (del 41–86) was detected with Ab 1. *C*, densitometry results for each construct expressed as the mean ± S.D. ratio of the P2 fraction to the sum of S2 and P2 fractions. *, significant difference at $p < 0.01$ when compared with FH969-18Q and $p < 0.001$ when compared with FH287-18Q ($n = 4$, ANOVA and *post hoc* Bonferroni test). *D*, immunofluorescent confocal microscopy of COS-1, clonal striatal (X57), and MCF-7 cells transiently expressing FH-287-18Q or FH171-18Q. Expressed protein was detected with anti-FLAG mAb M5. Scale bars, 5 μm. *E*, immunofluorescent confocal microscopy of MCF-7 cells expressing FH287-100Q and FH171-100Q. Expressed protein was detected with anti-FLAG mAb M5. Inset in bottom panel, confocal image of the same cell but through a plane at the top edge of the nucleus. Scale bars, 5 μm. *F*, mean percentage ± S.D. of FLAG-positive X57 cells with >50% PM staining assessed by immunofluorescent microscopy. *, significant difference compared with FH287-18Q at $p < 0.001$ ($n = 3$, ANOVA and *post hoc* Bonferroni test). *G*, mean percentage of FLAG-positive MCF-7 cells with >50% PM staining assessed by immunofluorescent microscopy. *, significant difference compared with FH287-18Q at $p < 0.001$ ($n = 3$, ANOVA and *post hoc* Bonferroni test).



sample cell, and calorimetric scans were performed by increasing the temperature at a rate of 30 °C/h. Data were collected at 0.05 °C intervals. The transition enthalpy, δH , of a normalized and base line-corrected thermogram was calculated as the numerically integrated area below the endotherm. The phase transition temperature, T_m , was defined as

the temperature at which the excess specific heat reaches a maximum. To describe the width of the gel to liquid-crystalline transition of lipid mixtures, the onset temperature of chain melting, T_s , which represents the solidus line, and the completion temperature of the chain melting, T_l , which represents the liquidus line, were determined.

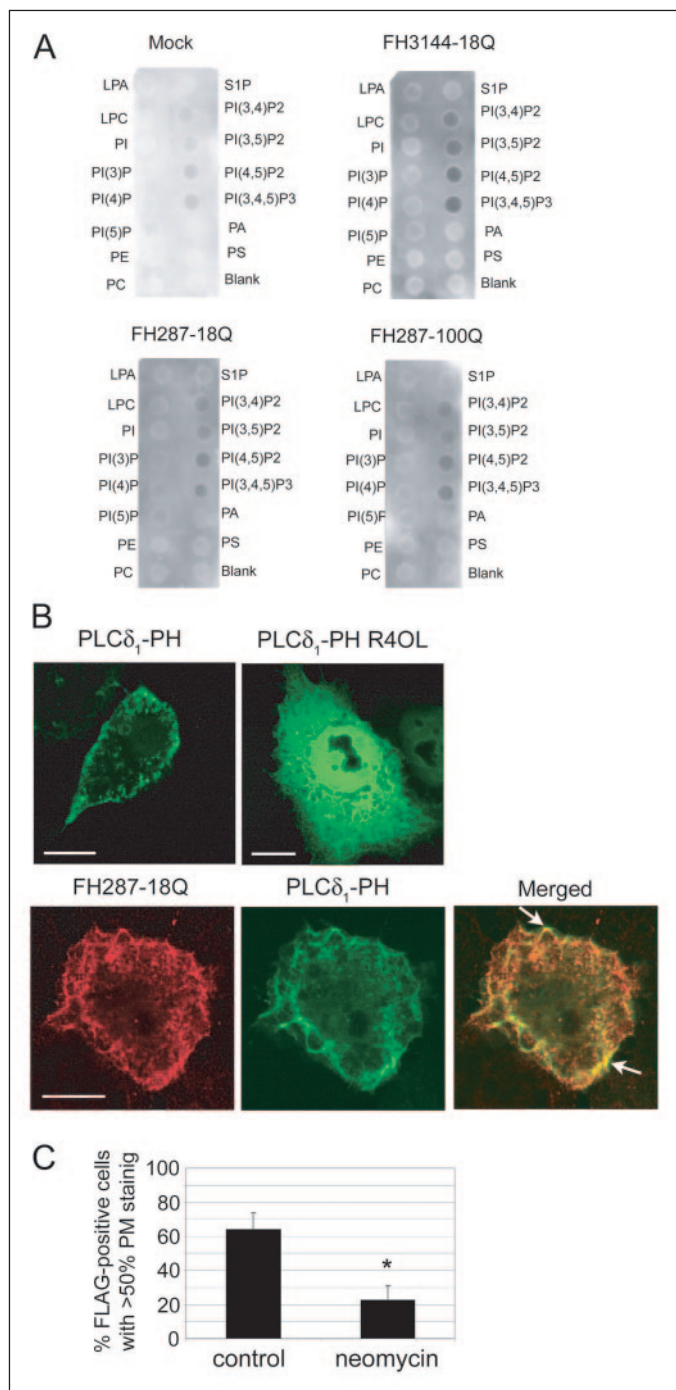


FIGURE 3. Analysis of htt association with acidic phospholipids. *A*, protein-lipid overlays. Postnuclear lysates from COS-1 cells expressing htt cDNAs as indicated were incubated with membranes spotted with various lipids (see "Materials and Methods" for details on lipids). Mock lysates, with endogenous htt, were prepared from COS-1 cells expressing pcDNA-FLAG. Blots were probed with anti-htt antibody Ab 1. *B*, PLC δ_1 -PH-GFP (*top left*) or PLC δ_1 -PH-GFP with an R40L mutation (*top right*) expressed in MCF-7 cells. *Bottom panel*, FH287-18Q (*red*) co-expressed with PLC δ_1 -PH-GFP (*green*). Co-localization (*arrows*) is shown in *yellow* (*Merged*). Scale bars, 5 μ m. *C*, mean percentage \pm S.D. of FLAG+ MCF-7 cells with >50% PM labeling. Transfected cells expressing FH287-18Q were treated for 18 h in complete medium (control) or with 10 mM neomycin in complete medium. *, significant difference at $p < 0.001$ ($n = 4$, two-tailed t test). LPA, lysophosphatidic acid; LPC, lysophosphatidylcholine; PI(3)P, PI 3-phosphate; PI(4)P, PI 4-phosphate; PI(5)P, PI 5-phosphate; PE, phosphatidylethanolamine; PC, phosphatidylcholine; S1-P, sphingosine 1-phosphate; PI(3,4)P2, PI 3,4-bisphosphate; PI(3,5)P2, PI 3,4-bisphosphate; PI(3,4,5)P3, PI 3,4,5-trisphosphate; PA, phosphatidic acid; PS, phosphatidylserine.

N-terminus Residues 1-171

```

1 matleklmka feslksfqqq qqqqqqqqqq qqqqqqqqqq
41 pppppppppp pqlpqqppqa qpllpqqppp pppppppppp
81 avaeeplhrp kkelsatkkd rvnhctice nivaqsvrns
121 pefqkllgia melfillcsdd aesdvrmvad eclnkvkikal
161 mdsnlprlql e
    
```

Residues 172-493

```

172 lykeikkng aprslraalw rfaelahlvr pqkcrpylvn
211 llpcltrtsk rpeesvqetl aaavpkimas fgnfandnei
251 kvllkafian lkssstirr taagsavsic qhsrrtqyfy
291 swllnvlgl lvpvedehst llilgvlltl rylvpllqqq
331 vkdtslkgsf gvtrkemevs psaeqlvqvy eltlhhtqhq
371 dhnvtgale llqqlfrtpp pellqtltav ggigqltaak
411 eesggrsrsg siveliaagg sscspvlsrk qkgkvllgee
451 ealedsser sdvssalta svkdeisgel aassgvstpg
491 sag
    
```

FIGURE 4. Primary sequence of the first 493 amino acids (of 3144 total) of wild-type htt. *Top*, the polyglutamine tract is in *boldface type*, the proline-rich region is in *italic type*, and amino acids that have hydrophilic, positively charged side groups (histidine, lysine, and arginine) are in *blue*. Shown with *boldface underline* is the region predicted to form an amphipathic helix (aa 229–246). The region from 1 to 171 is largely charge-neutral. The region from 172 to 448 is positively charged with 40 positive residues and 21 negative residues (glutamate and aspartate) and contains stretches of hydrophobicity.

Protein-Lipid Overlays—The protein overlay method was performed as described (16) using cell lysates (17). Homogenates from COS-1 cells expressing various htt constructs were prepared in 25 mM Tris (pH 7.4), 5 mM EDTA plus protease inhibitors (Mini mixture inhibitor (Roche Applied Science) plus 2 μ g/ml pepstatin A). Postnuclear supernatants were diluted to 60 or 500 μ g/ml in blocking buffer (TBST containing 3% fatty acid-free bovine serum albumin). Expression of exogenous htt was confirmed by Western blot. Membranes embedded with various phospholipids (PIP Strips; Molecular Probes) were incubated overnight at 4 $^{\circ}$ C in homogenates and then processed as described (16), using anti-htt Ab 1 (0.5 μ g/ml), mAb 1574 (1:5000; Chemicon), peroxidase-conjugated secondary antibody (1:10,000), and developed using ECL. All experiments were performed at least three separate times. Each spot contains 100 pmol of lipid and included lysophosphatidic acid, lysophosphatidylcholine, phosphatidylinositol (PI), PI 3-phosphate, PI 4-phosphate, PI 5-phosphate, phosphatidylethanolamine, phosphatidylcholine, sphingosine 1-phosphate, PI 3,4-bisphosphate, PI 3,5-bisphosphate, PI 4,5-bisphosphate (PI(4,5)P₂), PI 3,4,5-trisphosphate, phosphatidic acid, and phosphatidylserine.

Computer Analysis—htt aa 50–330 was submitted to a computational algorithm designed to identify/predict peptide sequences capable of lipid binding (Program SSCP version 2.0, revised September 1996) (18). htt 1–49 was omitted, because the polyglutamine stretch interfered with the analysis. The analysis seeks hydrophobic stretches that might form amphipathic helices and are flanked by regions rich in positive charge. (An amphipathic helix consists of three sectors: a hydrophobic sector that could incorporate into membranes and interact with the hydrophobic acyl tails of lipids, an interface region for lipid-head group interactions, and a polar sector that would be exposed to the aqueous cytosol.)

RESULTS

Biochemical Analysis of Membrane Association Domains in N-htt—Previous studies showed that normal endogenous htt, overexpressed full-length wild-type htt, and FH969-18Q distribute between membrane and soluble fractions in fractionated clonal striatal cells (5). We

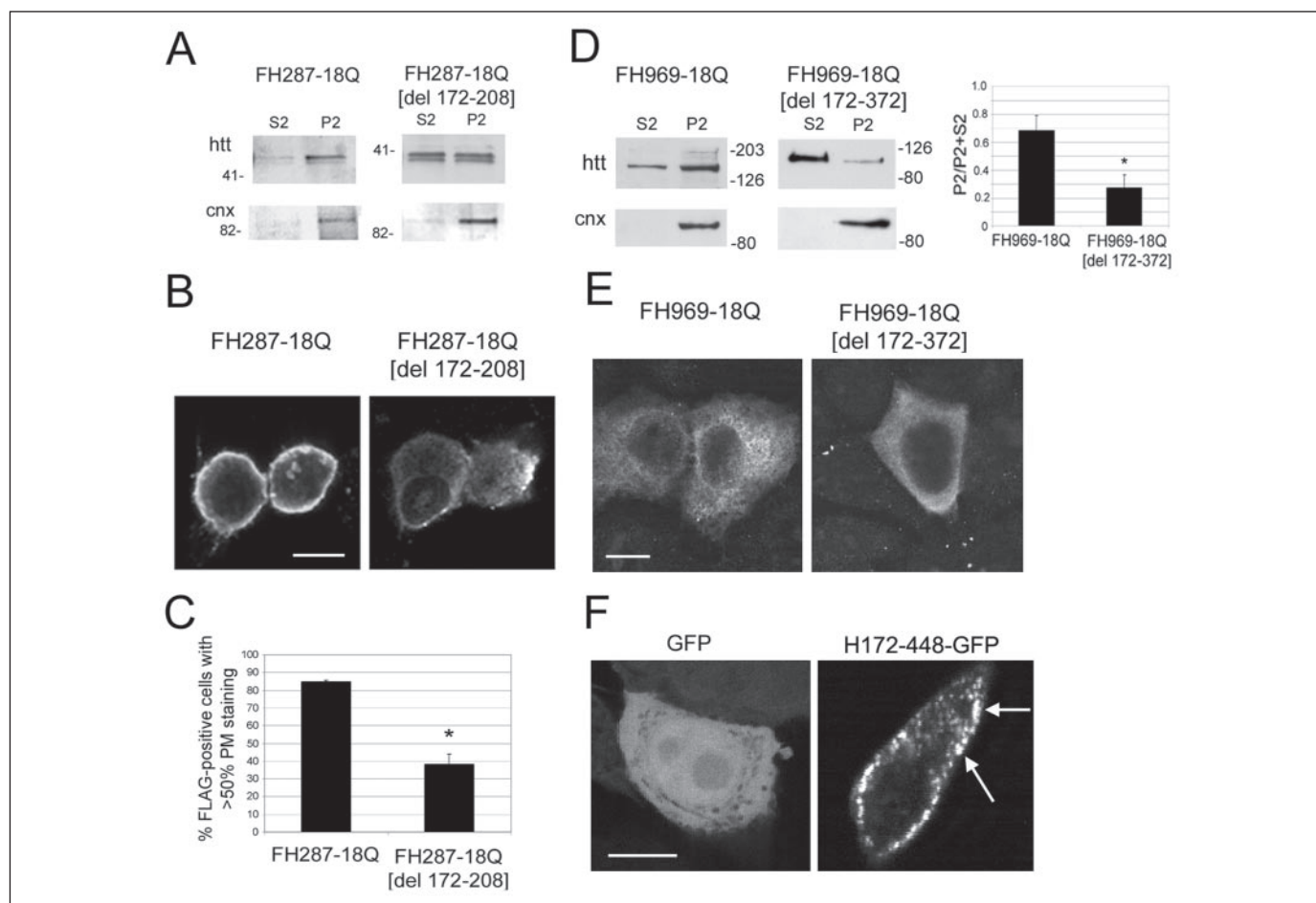


FIGURE 5. Biochemical and immunocytochemical analysis of expressed N-htt constructs containing deletions of positively charged residues. *A*, Western blots of subcellular fractions from COS-1 cells expressing FH287-18Q and FH287-18Q (del 172–208). Blots were probed with anti-huntingtin antiserum Ab 1 and reprobed with antiserum to calnexin, an endoplasmic reticulum marker. *B*, immunofluorescent confocal microscopy in clonal striatal cells of FH287-18Q and FH287-18Q (del 172–208). Expressed protein was detected using anti-FLAG monoclonal M5. Scale bars, 5 μ m. *C*, mean percentage \pm S.D. of FLAG+ clonal striatal cells expressing FH287-18Q or FH287-18Q (del 172–208) with >50% PM staining. *, significant difference at $p < 0.0001$ ($n = 3$, ANOVA and *post hoc* Bonferroni test). *D*, Western blots of subcellular fractions from COS-1 cells expressing FH969-18Q and FH969-18Q (del 172–372). Right, densitometry results shows mean ratio \pm S.D. of P2 fraction to the sum of S2 and P2 fractions. *, significant difference at $p < 0.05$ ($n = 4$, ANOVA and *post hoc* Bonferroni test). *E*, immunofluorescent confocal microscopy of MCF-7 cells expressing FH969-18Q and FH969-18Q (del 172–372) using anti-FLAG mAb M5. Scale bars, 5 μ m. *F*, fluorescent confocal microscopy of GFP and H172-448-GFP expressed in MCF-7 cells. H172-448-GFP localizes to patches on the plasma membrane (arrows) and on vesicles in the cytoplasm. Scale bars, 5 μ m.

performed subcellular fractionations of COS-1 cells transiently expressing a series of N-terminal FLAG-tagged htt constructs (Fig. 1). Results from several experiments in COS-1 cells showed FH969-18Q distributed partially in cytosolic (S2) and slightly more in the membrane (P2) fractions (Fig. 2A). FH493-18Q, FH400-18Q, and FH287-18Q had a similar distribution or were preferentially in the P2 fraction (Fig. 2A). FH232-18Q separated evenly in the S2 and P2 fractions (Fig. 2A). In contrast, FH171-18Q was more prevalent in the S2 fraction than the P2 fraction (Fig. 2A). Densitometry and statistical analysis of the soluble and membrane fractions revealed a statistically significant difference in cellular distribution for FH171-18Q compared with FH969-18Q ($p < 0.01$, $n = 4$, *post hoc* Bonferroni test) and compared with FH287-18Q ($p < 0.001$, $n = 4$, *post hoc* Bonferroni test) (Fig. 2C). Deletion of the proline region, FH969-18Q (del 41–86) and FH287-18Q (del 41–86), did not significantly affect the subcellular distribution of N-htt (Fig. 2, B and C). These findings suggest that a specialized domain for membrane binding occurs in the N-htt beyond residue 171.

Cellular Distribution of Expressed N-htt Proteins Assessed by Confocal Immunofluorescence—COS-1 cells expressing FH493-18Q, FH400-18Q, or FH287-18Q revealed FLAG immunoreactivity mainly in patches on the PM, with a small amount of diffuse staining occurring in

the cytoplasm (Fig. 2D, shown for FH287-18Q). FH287-18Q expression also showed PM staining in clonal striatal cells (X57), which have a neuronal phenotype, and in MCF-7 cells (Fig. 2D). In contrast, FH171-18Q was detected diffusely in the cytoplasm, in accord with biochemical results, and was present in cell nuclei (Fig. 2D). The number of transfected cells with >50% staining on the PM was significantly greater in cells expressing FH287-18Q than in those expressing FH171-18Q ($p < 0.001$, $n = 3$, *post hoc* Bonferroni) (Fig. 2, F and G). In agreement with the biochemical findings, these results also suggest that a specialized domain for membrane binding occurs in N-htt beyond residue 171. Furthermore, a targeting motif for directing htt to the PM may occur between htt 172 and 287.

Polyglutamine Expansion Prevents Normal Targeting of N-htt Fragments to the PM—To assess effects of polyglutamine expansion on the membrane targeting of htt, we expressed mutant N-htt, FH287-100Q, and FH171-100Q, in MCF-7 cells. FH287-100Q distributed to the perinuclear region or occurred diffusely in the cytoplasm (Fig. 2E). A significant reduction in cells with >50% PM staining was observed in cells expressing FH287-100Q compared with FH287-18Q ($p < 0.001$, $n = 3$, *post hoc* Bonferroni test) (Fig. 2G). Expressed FH171-100Q showed a similar distribution to FH287-100Q and was excluded from the

nucleus. A significant reduction of cells with >50% PM staining was also observed with FH171-100Q compared with FH287-18Q ($p < 0.001$, $n = 3$, *post hoc* Bonferroni test). Similar results were obtained in clonal striatal cells (data not shown). These data suggest that polyglutamine expansion prevents normal targeting of truncated htt 1–287 to the PM.

htt Binds to Acidic Phospholipids—To determine whether htt might bind directly to phospholipids, we performed protein-lipid overlays (16). Results showed that endogenous htt (mock), and overexpressed full-length htt (FH3144-18Q) and FH287-18Q associate with negatively charged (acidic) phospholipids (Fig. 3A). Acidic phospholipids included PI modified with one or two phosphate groups. At higher lysate concentrations (shown in Fig. 3A), htt showed an affinity for multivalent phospholipids including PI(4,5)P₂. At lower lysate concentrations, htt also bound to all phosphoinositides phosphates and to phosphatidylserine (data not shown).

Lysates from cells expressing mutant N-htt, FH969-100Q, or FH287-100Q, showed a similar pattern of lipid binding as their respective wild-type counterparts (Fig. 3A, shown for FH287-100Q). A monoclonal antibody specific for expanded polyglutamine tracts (mAb 1574) detected expressed mutant N-htt on the same set of lipids (data not shown). These results show that wild-type and mutant htt can associate with acidic phospholipids *in vitro*.

The acidic phospholipid PI(4,5)P₂ is enriched in the PM (19). When expressed in cells, the pleckstrin homology domain (a membrane binding motif) of the protein PLCδ₁ (PLCδ₁-PH) fused to GFP binds to PI(4,5)P₂ on the inner leaflet of the PM (20). Consistent with this observation, we found that PLCδ₁-PH-GFP targeted to the plasma membrane in MCF-7 cells; this localization was prevented by the mutation from arginine (positive) to leucine (neutral) of amino acid 40, which is essential for binding to PI(4,5)P₂ as previously described (20) (Fig. 3B, *top*). Co-expression of FH287-18Q with PLCδ₁-PH-GFP in MCF-7 cells showed co-localization of the two proteins (Fig. 3B, *bottom*), suggesting that in cells N-htt localizes to plasma membrane domains enriched in PI(4,5)P₂. Neomycin can bind and mask PI(4,5)P₂ in cells (21). Neomycin treatment of MCF-7 cells expressing FH287-18Q resulted in a significant reduction in the number of htt-positive cells with >50% PM staining ($p < 0.001$, $n = 4$, two-tailed *t* test) (Fig. 3C). Together, these data support the conclusion that htt associates with acidic phospholipids and can target to PI(4,5)P₂-enriched domains in cells.

Membrane Binding Regions of htt 50–330 Predicted by Computer Analysis—The region between amino acids 172 and 448 in htt is rich in positively charged residues (2:1 positive/negative) and hydrophobic residues (Fig. 4), a feature reminiscent of some lipid binding proteins such as talin (22). The residues between aa 172–448 encoding the positive charges are conserved in the rat, pig, mouse, zebrafish, and pufferfish htt sequences. An analysis of htt 50–330 using a computation algorithm designed to identify membrane binding regions (18) revealed that htt segments 174–221 and 250–285 have a high number of positively charged residues that could bind to membranes by electrostatic interactions with negatively charged phospholipids. The analysis also identified an intervening region (aa 229–246) enriched in hydrophobic residues predicted to form an amphipathic helix, a structure capable of membrane insertion (Fig. 4). The amphipathic helix region is conserved in rat, pig, and mouse; in zebrafish and pufferfish, two changes corresponding to S240A and F241L in the human sequence and a nonconservative change of N243H still encode an amphipathic helix. In addition, the secondary structure of htt 50–330 was predicted to be highly α-helical (93%), which can facilitate membrane binding.

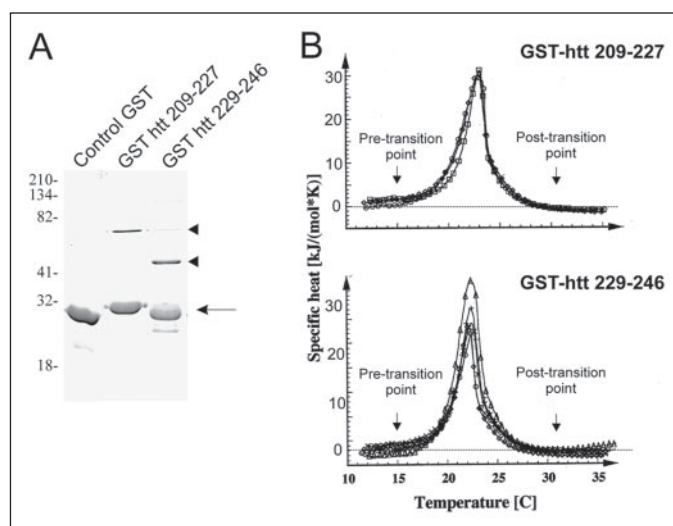


FIGURE 6. Differential scanning calorimetry with purified GST-htt peptides. A, Coomassie gels showing purity of GST fusion proteins migrating as monomers (arrow) and dimers (arrowheads). Molecular mass is indicated in kDa on the left. The higher molecular mass products (arrowheads) were confirmed to be dimers by Western blot analysis. The hydrophobic nature of GST-htt 229–246 may explain its faster mobility on SDS-PAGE compared with GST-htt 209–229. B, differential scanning calorimetry heating profiles of pure reconstituted dimyristoyl-L- α -phosphatidylcholine/dimyristoyl-L- α -phosphatidylglycerol vesicles (1 mg/ml, 70:30 molar ratio, 200-nm diameter) with fusion protein GST-htt 209–227 (*top*) and GST-htt 229–246 (*bottom*). The control, no GST protein, or 20 μ M GST plus dimyristoyl-L- α -phosphatidylcholine/dimyristoyl-L- α -phosphatidylglycerol vesicles (1:40 protein/lipid), is shown on each graph (*top*, squares; *bottom*, triangles). Protein/lipid molar ratio of test peptide in *top*, 1:400; in *bottom*, 1:2000, 1:400, 1:200, and 1:40.

htt Binding to Cellular Membranes Requires Positively Charged Regions Flanking the Amphipathic Helix in htt—Our analysis showed that FH232-F18Q was partially removed from membranes compared with FH287-18Q (Fig. 2A). FH232-18Q lacks much of the predicted amphipathic helix (aa 229–246) and all of the distal, positively charged region (aa 250–285) present in htt 1–287. To test the contribution of the positively charged region preceding the amphipathic helix in membrane association, we deleted aa 172–208 in FH287-18Q. FH287-18Q (del 172–208) distributed slightly more to the cytosolic fraction (S2) than to FH287-18Q (Fig. 5A). The mean percentage of cells with >50% PM staining was significantly less in cells expressing FH287-18Q (del 172–208) compared with cells with FH287-18Q ($p < 0.001$, $n = 3$, Bonferroni test) (Fig. 5, B and C). Quantitative analysis of the biochemical distribution and cellular localization of FH287-18Q (aa 229–246), which deletes the amphipathic helix, was similar to FH287-18Q (data not shown). Altogether, these data suggest that the cationic regions flanking the amphipathic helix make a major contribution of htt binding to membranes.

We found that deletion of aa 172–208 in FH969-18Q was insufficient to affect membrane localization following differential centrifugation (data not shown), confirming that additional sequences within htt 209–969 contribute to membrane binding. Therefore, we deleted aa 172–372, which includes the first three HEAT repeats (aa 205–329) plus a stretch of 43 residues that contains a hydrophobic region followed by positive charges, including a cluster of histidines (aa 365–369). Subcellular fractionation and densitometry analysis showed that FH969-18Q (del 172–372) was significantly more distributed to the soluble fraction (S2) than FH969-18Q ($p < 0.05$, $n = 4$, Bonferroni test) (Fig. 5D). Residual membrane binding was possibly due to the remaining cluster of 4 positive residues between aa 439 and 444; alternatively, residual binding may be due to protein-protein interactions. Confocal immunofluorescence shows that FH969-18Q (del 172–372) was more diffuse through-

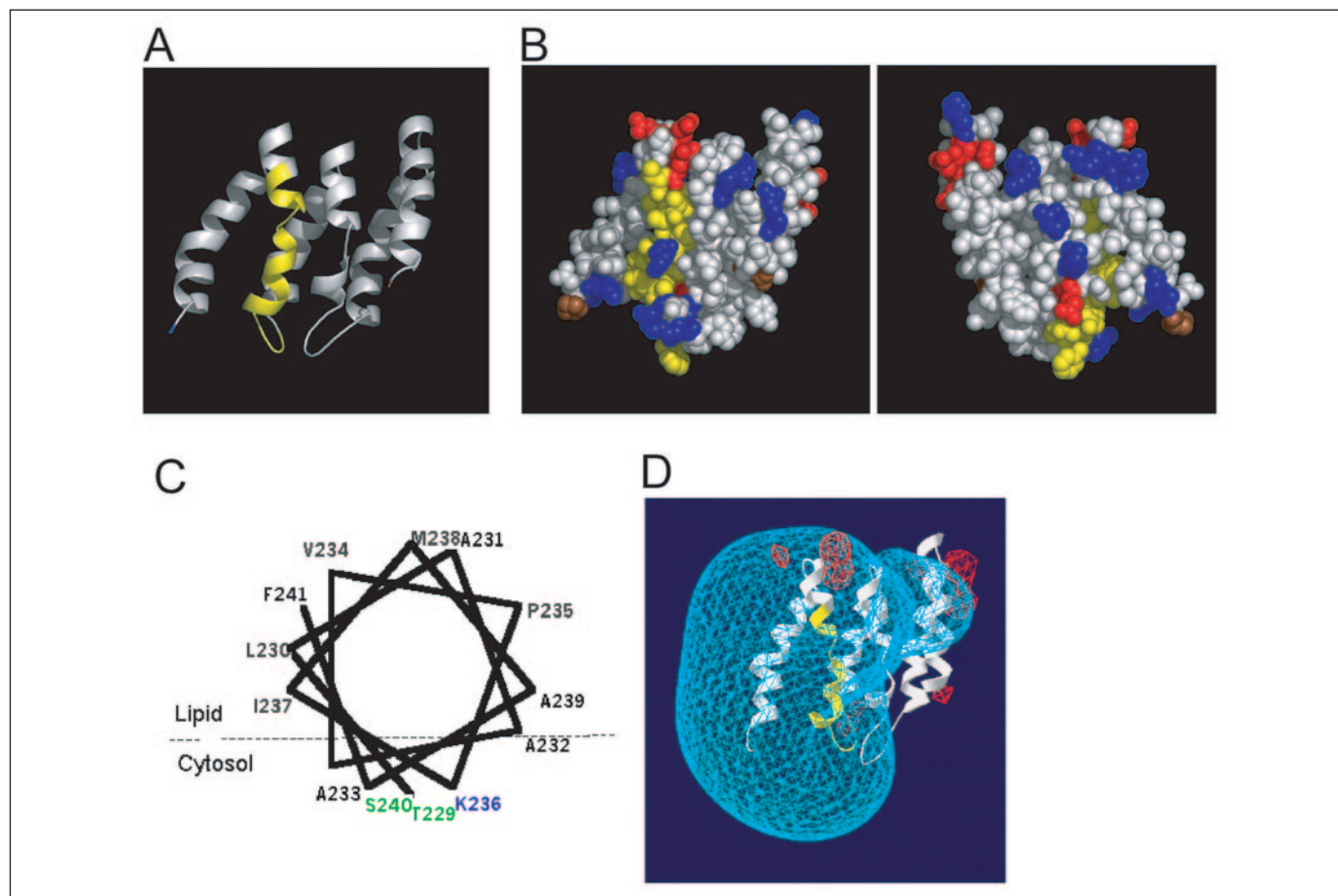


FIGURE 7. *A*, three-dimensional model for htt residues 201–327 based on homology modeling with the crystalline coordinates from protein phosphatase 2A PR65/A. The consecutive three HEAT repeats are each composed of paired α -helices. The second helices of the first two repeats are interrupted in their midsections, producing a kink in the overall alignment. The region that can insert into synthetic lipid vesicles (residues 229–246) is colored yellow, the amino terminus is shown in blue, and the carboxyl terminus is shown in red. *B*, space-filling representations of *A* demonstrate the distribution of charge groups. Negatively charged residues (Asp and Glu) are colored red, positively charged amino acids are colored blue (His, Lys, and Arg), and the amino/carboxyl termini are indicated in brown. The model on the left is oriented identically to that in *A*, whereas the right model has been rotated 180° around the vertical axis. *C*, helical wheel representation of htt segment 229–241 as an amphipathic helix. Although shown here as a continuous helix, homology modeling with the HEAT repeats of the protein phosphatase 2A PR65/A suggests that only htt residues 229–231 and 235–241 are true α -helix (as in *A*). Intercalated residues 232–234 form a distorted helix-type structure that may be conformationally flexible. The dashed line demarcates the hypothetical boundary between lipid and cytosol; hydrophobic residues (black) on the top surface of the helix would interact with the hydrophobic acyl chains of the phospholipids, whereas neutral, charged (blue), and polar residues (green) would interact with the polar head groups of phospholipids and aqueous cytosol. The wheel was drawn with the assistance of WinPep (38). *D*, electrostatic potential map for htt residues 201–327 with residues 229–246 shown in yellow. A large distribution of positive potential may account for the preference of htt for anionic phospholipids. The potential map was calculated with Deep View, The Swiss-PdbViewer, using the Coulomb method with a solvent dielectric constant of 80. The map is contoured at -1.80 kT/e (red) < 0.0 kT/e (white) < 1.80 kT/e (blue) (39), where k is the Boltzmann constant, T is the absolute temperature, and e , is the charge of a proton.

out the cytoplasm compared with FH969–18Q (Fig. 5E). FH969–18Q (del 172–373) also failed to bind efficiently to acidic phospholipids in a protein-lipid overlay (data not shown). These results show that regions in htt rich in positively charged side chains present between aa 172 and 373 and flanking aa 229–246 contribute to membrane binding. This region includes the first three HEAT repeats in htt.

Finally, we created a cDNA fusion encoding htt 172–448 fused to GFP (H172–448-GFP). In MCF-7 cells, fluorescence microscopy showed that H172–448-GFP was diffuse in the cytoplasm and also localized to vesicles and the PM (Fig. 5F). These results show that htt residues 172–448 are sufficient for membrane association.

A htt Peptide Can Insert into Pure Lipid Bilayers—Although the predicted amphipathic helix (aa 229–246) was not necessary for membrane association, its insertion into the membrane could serve to anchor htt to the lipid bilayer after association. In differential scanning calorimetry, a reduction in the specific heat necessary to bring about a phase transition provides evidence of membrane insertion. GST, GST-htt 209–227 (negative control), and GST-htt 229–246 (test peptide), were purified and tested (Fig. 6). Addition of

GST-htt 229–246 altered the thermotropic properties of lipid vesicles in a dose-dependent manner (Fig. 6B, bottom), whereas the addition of GST or GST-htt 209–227 (Fig. 6B, top) had no effect. The endotherm for GST-htt 229–246 shows a variation of the pretransition and main phase transition with increasing protein concentration. Increasing the protein concentration of GST-htt 229–246 decreased the heating profile from pretransition point to post-transition point. The suppression of δH (enthalpy) and the broadening of the phase transition by GST-htt 229–246 indicate protein insertion. These results show that aa 229–246 in htt can insert into pure lipid bilayers and may help anchor htt to membranes.

Molecular Model of the htt Putative Membrane Interaction Region—There is no available NMR or crystallographic data of the structure of htt. Nevertheless, we tried to place our biochemical and physical data for htt in a structural context. We found the first three HEAT repeats in htt important for membrane binding. Thus, we generated a three-dimensional structure of htt (Fig. 7) based on sequence and HEAT motif homology to the crystallographically determined structure of the protein phosphatase 2A PR65/A (10, 23), another HEAT-containing pro-

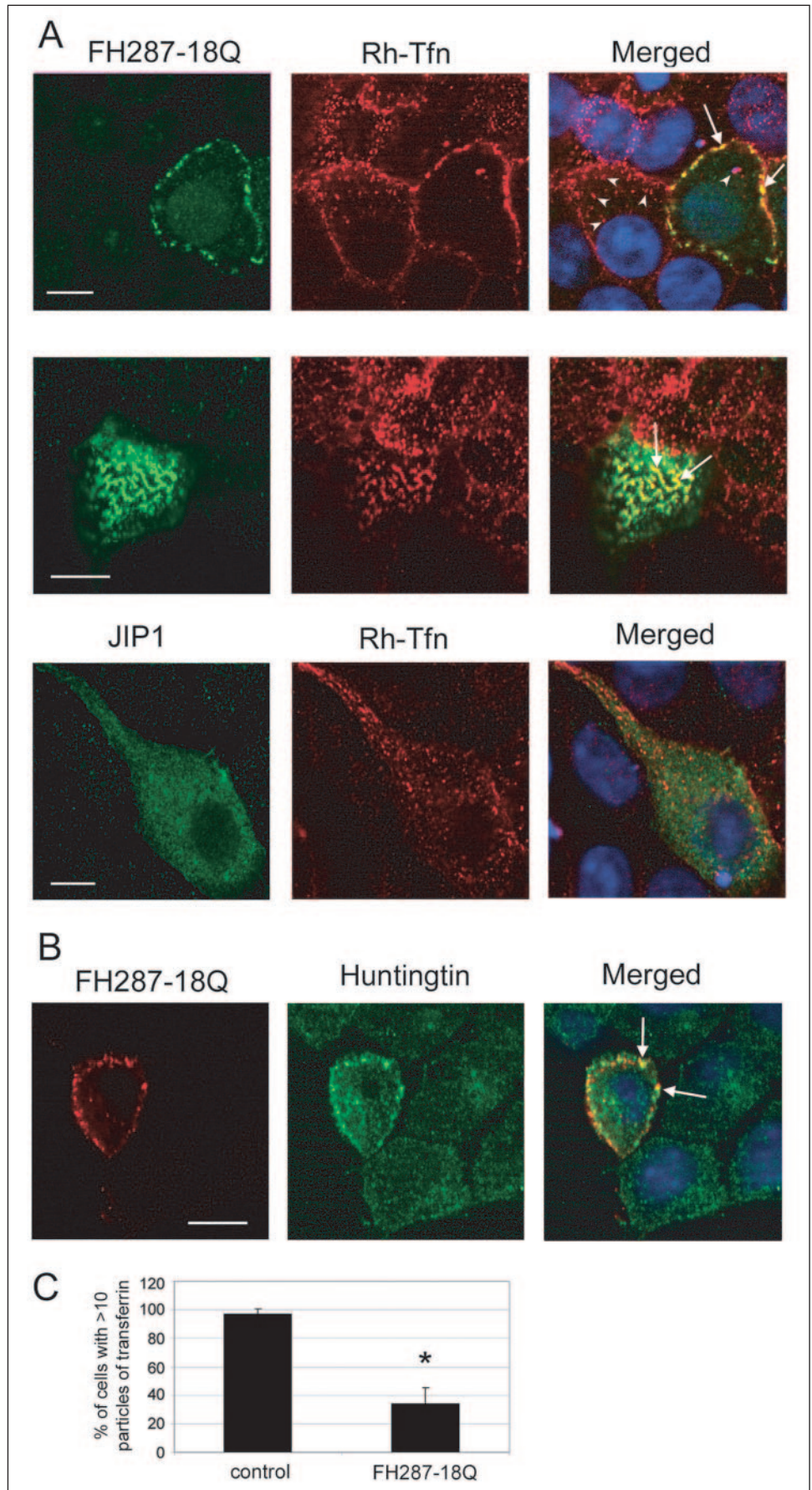


FIGURE 8. Localization of N-htt and transferrin. *A, top panel*, MCF-7 cells expressing FH287-18Q (green) and rhodamine-transferrin (red) co-localize (yellow, merged) in patches at the plasma membrane (arrows). Internalized transferrin (arrowheads) is less abundant in FLAG-positive cells compared with FLAG-negative cells in the same field. *Middle panel*, in some cells, large submembrane patches were observed (arrows). *Bottom panel*, exogenous c-Jun N-terminal kinase-interacting protein 1 does not form patches at the plasma membrane and does not alter transferrin internalization. FLAG was detected with monoclonal antibody M5 and in *B*. Scale bars, 5 μ m. *B*, endogenous htt detected with antiserum against htt 585–725 co-localizes with FH287-18Q in patches on the plasma membrane (arrows) in a transfected X57 cell. Scale bars, 5 μ m. Nuclei in *A* and *B* were stained with Hoechst (blue). *C*, mean percentage \pm S.D. of MCF-7 cells with >10 visible spots of transferrin. FLAG-positive cells, expressing FH287-18Q, were compared with FLAG-negative cells on the same coverslip. *, significant difference at $p < 0.001$ ($n = 4$, two-tailed t test).

Huntingtin Associates with Acidic Phospholipids

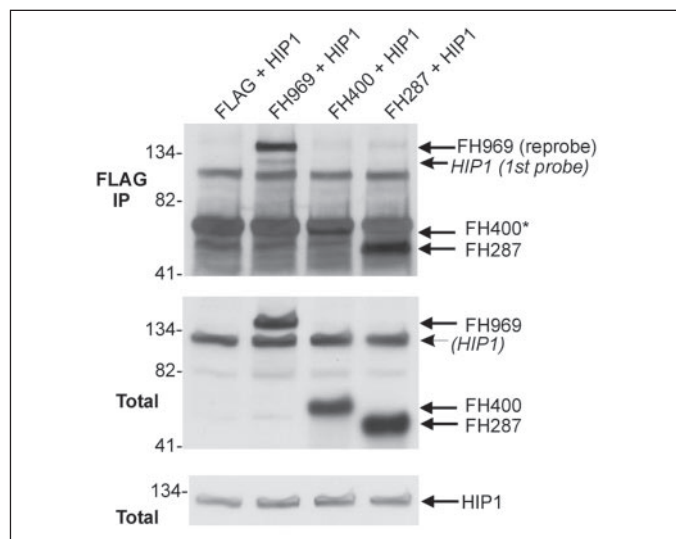


FIGURE 9. htt-HIP1 co-immunoprecipitations. *Top*, Western blot of immunoprecipitates (IP) isolated using anti-FLAG mAb M2 from transfected COS-1 cells expressing the indicated proteins. Blot was probed with anti-HIP1 mAb to detect co-immunoprecipitated HIP1 and then reprobated with Ab 1 to confirm pull-down of FH969, FH400, and FH287. *, FH400-18Q is pulled down but is partially obscured by the IgG signal. The *top* blot shows HIP1 pulled down only by FH969-18Q. *Middle and bottom panels*, Western blots of total lysates. One-tenth volume of input lysate is present per lane. The blot was probed first with anti-HIP1 mAb (*bottom*) and then reprobated with anti-htt antiserum Ab 1 to confirm expression levels of FH969, FH400, and FH287 (*middle*).

tein. Trials using multiple sequence alignment programs failed to identify an appropriate starting model for the amino-terminal segment of the binding region in htt (residues 172–200), and these residues are absent from the final model (residues 201–327). The model suggests that residues 229–246, which we showed can insert into pure lipid vesicles, contribute to the formation of a bipartite α -helix (residues 229–241) as well as a carboxyl-terminal extended loop (residues 242–246) (shown in yellow in Fig. 7, *A* and *B*). Only residues 229–231 and 235–241 of htt are true α -helix; intercalated residues 232–234 form a distorted helix-type structure that may be conformationally flexible. The predicted helix is amphipathic as expected for a structure implicated in mediating membrane association (Fig. 7*C*). A calculation of the associated electrostatic potentials for the entire peptide (residues 201–327) reveals a robust positive potential that envelops the predicted membrane binding domain (Fig. 7*D*), consistent with our previous results showing that htt binds anionic phospholipids (Fig. 3). Although the model only incorporates 127 amino acids of the intact huntingtin (3144 residues), our structural predictions are consistent with an electrostatic mechanism of binding to lipids.

Characterization of htt-positive Patches on the PM—PI(4,5)P₂ is essential for recruitment of AP-2 and clathrin-mediated endocytosis (24, 25). In adipocytes, the PLC δ 1-PH domain localized with labeled transferrin in discrete PM domains, which are considered to be zones of endocytosis (26). FH287-18Q also colocalized with patches of rhodamine-transferrin on the cell surface (Fig. 8*A*, *top*) and in submembrane patches at the top edge of cells (Fig. 8*A*, *middle*). No co-localization was seen with transferrin and an exogenously expressed control protein, c-Jun N-terminal kinase-interacting protein 1, which distributed diffusely in the cytoplasm (Fig. 8*A*, *bottom*). Moreover, endogenous htt also accumulated with FH287-18Q in some PM patches (Fig. 8*B*), implying that binding of FH287-18Q to the PM represents a normal targeting event for wild-type htt. Cells with patches formed by FH287-18Q had significantly less internalized rhodamine-transferrin compared with untransfected cells ($p < 0.001$, $n = 4$, two-tailed t test) (Fig.

8*C*). These results show that FH287-18Q may represent a dominant negative form of wild-type htt capable of blocking normal function.

Analysis of htt 1–287 and htt 1–969 Interactions with HIP1—HIP1 is an endocytic accessory protein that co-purifies with htt on clathrin-coated vesicles (27), is capable of binding phosphoinositides (28, 29), and can recruit AP-2 and clathrin to membranes (27, 29). HIP1 was identified in a yeast two-hybrid screen using as bait htt 1–588 (30) or htt 1–540 (31). To determine whether an interaction with HIP1 was necessary for htt to interact with membranes, we performed coimmunoprecipitations with cells transiently expressing HIP1 and either FH287-18Q, FH400-18Q, or FH969-18Q. HIP1 interacts with FH969-18Q but not with FH287-18Q or FH400-18Q (Fig. 9). The results suggest that interactions with HIP1 are not essential for association of htt 1–287 with membranes.

DISCUSSION

We have defined a protein domain in N-htt, aa 172–372, important for membrane association and responsible for targeting wild-type N-htt products to the PM. This region may also target full-length wild-type htt to the PM. Structural predictions of this region are consistent with direct membrane binding through electrostatic interactions with acidic phospholipids. Localization of htt to transferrin-positive/PI(4,5)P₂-enriched patches at the PM is consistent with the idea that wild-type htt is involved in endocytosis. Polyglutamine expansion overrides PM targeting of N-htt.

Mechanism of Membrane Association—Our data show that a region in N-htt containing multiple basic residues contributes to membrane association. Furthermore, we found that htt binds to negatively charged phospholipids in protein-lipid overlay assays. The helical HEAT domain in htt that mediates membrane association is similar to epsin N-terminal homology domains, which occur in epsin (32) and AP180 (33). These α -helical superhelical solenoids use an electrostatic mechanism to bind membranes; in the case of epsin, an amphipathic helix has been shown to order upon binding to the membrane (34). Our measurements with differential scanning calorimetry showed that the fusion protein GST-htt 229–246 encoding the predicted amphipathic helix inserts into negatively charged phospholipid membranes. However, deletion of aa 229–246 in htt did not alter binding to membranes, whereas deletion of basic regions on either side did. We hypothesize that htt first binds to acidic phospholipids through an electrostatic interaction using the basic side groups of positive residues; the flexible, amphipathic helix then may partially penetrate into the bilayer to form an anchor. Other lipid binding proteins that primarily use electrostatic mechanisms to bind membranes embed hydrophobic helices (vinculin) or a hydrophobic loop (FYVE and PX domain proteins) into the lipid bilayer to form an anchor (34, 35). In htt, the phenylalanine at residue 244 predicted to lie within an extended loop (aa 242–246) could also insert its hydrophobic side group into the bilayer to provide an anchor. Since htt is a soluble protein, it may undergo a molten globule (partially unfolded) state in order to form a stable association with the membrane, similar to other proteins (36).

Our results are consistent with direct binding of N-htt 172–372 to membranes through electrostatic interactions; other mechanisms of membrane binding are also possible for this domain. For instance, the region we have defined could be a protein-binding module that allows htt to bind a membrane-associated protein other than HIP1.

Binding to Specific Lipids and Targeting to Specific Membranes—Analysis by protein-lipid overlay showed that htt associates with many phosphoinositol phosphates. Consistent with this result, htt has been detected on many types of membranes in cells, each of which contain

different phospholipids (1–3). For example, present at the PM is PI(4,5)P₂, on many endosomes PI 3-phosphate is found, and Golgi membranes are enriched in PI 4-phosphate (19). Similar to other proteins, htt may partner with other proteins to create specificity and increase binding affinity (19).

We do not know why an altered affinity/specificity for particular phosphoinositides and for phosphatidylserine was observed in the protein-lipid overlay experiments with higher *versus* lower lysate concentrations. Further studies will be required to determine whether htt at higher concentrations dimerizes with itself or another protein to create specific interactions or altered binding affinities.

Normal htt Function at the PM—FH287-18Q colocalized with the endocytic cargo transferrin and with PI(4,5)P₂ at patches in the PM. PI(4,5)P₂ is essential for plasma membrane recruitment of the endocytic protein AP-2 and for clathrin-mediated endocytosis (24, 25). Endogenous htt has been detected on coated vesicles near the plasma membrane using immunofluorescence (3) and together with HIP1 on clathrin-coated vesicles purified from brain (27). Immunogold EM showed FH969-18Q on clathrin-coated invaginations on the PM in clonal striatal cells (5). These observations are consistent with the idea that htt functions in endocytosis. Through direct interaction with PI(4,5)P₂, htt is positioned to act as a scaffold for recruiting other endocytic proteins to membrane surfaces or for stabilizing protein complexes.

The block observed in transferrin internalization with expression of htt 1–287 might be due to an inability of htt 1–287 to recruit endocytic machinery compared with full-length htt. Alternatively, htt 1–287 may saturate potential sites for receptor-mediated transferrin endocytosis and compete with other PI(4,5)P₂ binding proteins required for endocytosis. Inhibition of transferrin internalization was also observed in adipocytes expressing PLCδ₁-PH domain, which accumulated in large membrane patches (26).

Relevance to HD—Our results show that polyglutamine expansion disrupted N-htt localization to the PM. We found no difference in binding of wild-type or mutant N-htt fragments in lipid overlay experiments that might explain the mistargeting of mutant N-htt to the perinuclear region. However, conclusions based on these experiments must be limited, since different pools of mutant htt with altered confirmations probably exist in cells. We cannot be certain that the soluble postnuclear supernatant used in the overlay assay contained the mistargeted fragments observed in cells. Alternatively, mutant N-htt may have a higher affinity for itself than for phospholipids producing perinuclear aggregates or prefer binding to an interactor protein, which alters mutant N-htt localization.

Normal breakdown of some proteins requires localization to the plasma membrane. For instance, the yeast G protein α subunit Gpa1 is normally degraded through the vacuolar (lysosomal-like) pathway following monoubiquitination at the plasma membrane (37). N-terminal htt fragments are degraded through endosomal-lysosomal and autophagic pathways (5, 6). We speculate that htt may require localization at the plasma membrane to receive modification for targeting to clearance pathways. By preventing targeting of N-terminal mutant htt fragments to the plasma membrane, polyglutamine expansion may impede protein degradation and thereby contribute to HD pathogenesis.

Acknowledgments—We thank Shaohui Huang and Michael P. Czech (University of Massachusetts Medical School, Worcester, MA) for normal and mutant PLCδ₁-PH-GFP and Dr. R. J. Davis (Howard Hughes Medical Institute, University of Massachusetts Medical School, Worcester, MA) for c-Jun N-terminal kinase-interacting protein 1 cDNA.

REFERENCES

- DiFiglia, M., Sapp, E., Chase, K., Schwarz, C., Meloni, A., Young, C., Martin, E., Vonsattel, J. P., Carraway, R., Reeves, S. A., Boyce, F. M., and Aronin, N. (1995) *Neuron* **14**, 1075–1081
- Sharp, A. H., Loev, S. J., Schilling, G., Li, S. H., Li, X. J., Bao, J., Wagster, M. V., Kotzduk, J. A., Steiner, J. P., Lo, A., Hedreen, J., Sisodia, S., Snyder, S. H., Dawson, T. M., Ryugo, D. K., and Ross, C. A. (1995) *Neuron* **14**, 1065–1074
- Velier, J., Kim, M., Schwarz, C., Kim, T. W., Sapp, E., Chase, K., Aronin, N., and DiFiglia, M. (1998) *Exp. Neurol.* **152**, 34–40
- Harjes, P., and Wanker, E. E. (2003) *Trends Biochem. Sci.* **28**, 425–433
- Kegel, K. B., Kim, M., Sapp, E., McIntyre, C., Castano, J. G., Aronin, N., and DiFiglia, M. (2000) *J. Neurosci.* **20**, 7268–7278
- Qin, Z. H., Wang, Y., Kegel, K. B., Kazantsev, A., Apostol, B. L., Thompson, L. M., Yoder, J., Aronin, N., and DiFiglia, M. (2003) *Hum. Mol. Genet.* **12**, 3231–3244
- Kim, Y. J., Yi, Y., Sapp, E., Wang, Y., Cuiffo, B., Kegel, K. B., Qin, Z. H., Aronin, N., and DiFiglia, M. (2001) *Proc. Natl. Acad. Sci. U. S. A.* **98**, 12784–12789
- Szebenyi, G., Morfini, G. A., Babcock, A., Gould, M., Selkoe, K., Stenoien, D. L., Young, M., Faber, P. W., MacDonald, M. E., McPhaul, M. J., and Brady, S. T. (2003) *Neuron* **40**, 41–52
- Andrade, M. A., and Bork, P. (1995) *Nat. Genet.* **11**, 115–116
- Groves, M. R., Hanlon, N., Turowski, P., Hemmings, B. A., and Barford, D. (1999) *Cell* **96**, 99–110
- Wainwright, M. S., Perry, B. D., Won, L. A., O'Malley, K. L., Wang, W. Y., Ehrlich, M. E., and Heller, A. (1995) *J. Neurosci.* **15**, 676–688
- Kim, M., Lee, H. S., LaForet, G., McIntyre, C., Martin, E. J., Chang, P., Kim, T. W., Williams, M., Reddy, P. H., Tagle, D., Boyce, F. M., Won, L., Heller, A., Aronin, N., and DiFiglia, M. (1999) *J. Neurosci.* **19**, 964–973
- Morrison, D. K., and Davis, R. J. (2003) *Annu. Rev. Cell Dev. Biol.* **19**, 91–118
- Kegel, K. B., Meloni, A. R., Yi, Y., Kim, Y. J., Doyle, E., Cuiffo, B. G., Sapp, E., Wang, Y., Qin, Z. H., Chen, J. D., Nevins, J. R., Aronin, N., and DiFiglia, M. (2002) *J. Biol. Chem.* **277**, 7466–7476
- Tempel, M., Goldmann, W. H., Dietrich, C., Niggli, V., Weber, T., Sackmann, E., and Isenberg, G. (1994) *Biochemistry* **33**, 12565–12572
- Stevenson, J. M., Perera, I. Y., and Boss, W. F. (1998) *J. Biol. Chem.* **273**, 22761–22767
- Okamoto, Y., Vaena De Avalos, S., and Hannun, Y. A. (2002) *J. Biol. Chem.* **277**, 46470–46477
- Tempel, M., Goldmann, W. H., Isenberg, G., and Sackmann, E. (1995) *Biophys. J.* **69**, 228–241
- Wenk, M. R., and De Camilli, P. (2004) *Proc. Natl. Acad. Sci. U. S. A.* **101**, 8262–8269
- Varnai, P., and Balla, T. (1998) *J. Cell Biol.* **143**, 501–510
- Laux, T., Fukami, K., Thelen, M., Golub, T., Frey, D., and Caroni, P. (2000) *J. Cell Biol.* **149**, 1455–1472
- Seelig, A., Blatter, X. L., Frentzel, A., and Isenberg, G. (2000) *J. Biol. Chem.* **275**, 17954–17961
- Schwede, T., Kopp, J., Guex, N., and Peitsch, M. C. (2003) *Nucleic Acids Res.* **31**, 3381–3385
- Gaidarov, I., and Keen, J. H. (1999) *J. Cell Biol.* **146**, 755–764
- Padron, D., Wang, Y. J., Yamamoto, M., Yin, H., and Roth, M. G. (2003) *J. Cell Biol.* **162**, 693–701
- Huang, S., Lifshitz, L., Patki-Kamath, V., Tuft, R., Fogarty, K., and Czech, M. P. (2004) *Mol. Cell Biol.* **24**, 9102–9123
- Waelter, S., Scherzinger, E., Hasenbank, R., Nordhoff, E., Lurz, R., Goehler, H., Gaus, C., Sathasivam, K., Bates, G. P., Lehrach, H., and Wanker, E. E. (2001) *Hum. Mol. Genet.* **10**, 1807–1817
- Hyun, T. S., Rao, D. S., Saint-Dic, D., Michael, L. E., Kumar, P. D., Bradley, S. V., Mizukami, I. F., Oravec-Wilson, K. L., and Ross, T. S. (2004) *J. Biol. Chem.* **279**, 14294–14306
- Mishra, S. K., Agostinelli, N. R., Brett, T. J., Mizukami, I., Ross, T. S., and Traub, L. M. (2001) *J. Biol. Chem.* **276**, 46230–46236
- Wanker, E. E., Rovira, C., Scherzinger, E., Hasenbank, R., Walter, S., Tait, D., Colicelli, J., and Lehrach, H. (1997) *Hum. Mol. Genet.* **6**, 487–495
- Kalchman, M. A., Koide, H. B., McCutcheon, K., Graham, R. K., Nichol, K., Nishiyama, K., Kazemi-Esfarjani, P., Lynn, F. C., Wellington, C., Metzler, M., Goldberg, Y. P., Kanazawa, I., Gietz, R. D., and Hayden, M. R. (1997) *Nat. Genet.* **16**, 44–53
- Hyman, J., Chen, H., Di Fiore, P. P., De Camilli, P., and Brunger, A. T. (2000) *J. Cell Biol.* **149**, 537–546
- Mao, Y., Chen, J., Maynard, J. A., Zhang, B., and Quijcho, F. A. (2001) *Cell* **104**, 433–440
- Lemmon, M. A. (2003) *Traffic* **4**, 201–213
- Niggli, V. (2001) *Trends Biochem. Sci.* **26**, 604–611
- Banuelos, S., and Muga, A. (1995) *J. Biol. Chem.* **270**, 29910–29915
- Wang, Y., Marotti, L. A., Jr., Lee, M. J., and Dohlman, H. G. (2005) *J. Biol. Chem.* **280**, 284–291
- Hennig, L. (1999) *BioTechniques* **26**, 1170–1172
- Guex, N., and Peitsch, M. C. (1997) *Electrophoresis* **18**, 2714–2723